Accurate time propagation for the Schrodinger equation with an explicitly time-dependent Hamiltonian

Article *in* The Journal of Chemical Physics · June 2008

DOI: 10.1063/1.2916581 · Source: PubMed

3 authors, including:

Sverker Holmgren
Uppsala University
72 PUBLICATIONS **604** CITATIONS
SEE PROFILE

Hans O Karlsson
Uppsala University
75 PUBLICATIONS **578** CITATIONS
SEE PROFILE

Accurate time propagation for the Schrödinger equation with an explicitly time-dependent Hamiltonian

Katharina Kormann, Sverker Holmgren, and Hans O. Karlsson

Citation: J. Chem. Phys. **128**, 184101 (2008); doi: 10.1063/1.2916581
View online: http://dx.doi.org/10.1063/1.2916581
View Table of Contents: http://jcp.aip.org/resource/1/JCPSA6/v128/i18
Published by the AIP Publishing LLC.

Accurate time propagation for the Schrödinger equation with an explicitly time-dependent Hamiltonian

Katharina Kormann,[1] Sverker Holmgren,[1] and Hans O. Karlsson[2,a)]
[1]*Division of Scientific Computing, Department of Information Technology, Uppsala University, Box 337, SE-751 05 Uppsala, Sweden*
[2]*Quantum Chemistry, Department of Physical and Analytical Chemistry, Uppsala University, Box 518, SE-751 20 Uppsala, Sweden*

(Received 4 March 2008; accepted 3 April 2008; published online 8 May 2008)

Several different numerical propagation techniques for explicitly time-dependent Hamiltonians are discussed and compared, with the focus on models of pump-probe experiments. The quality of the rotating wave approximation is analyzed analytically, and we point out under which circumstances the modeling becomes inaccurate. For calculations with the fully time-dependent Hamiltonian, we show that for multistate systems, with either time or space dependence in the interstate coupling, the fourth order truncated Magnus expansion can be reformulated so that no commutators appear. Our results show that the split-operator method should only be used when low accuracy is acceptable. For accurate and efficient time stepping, the Magnus-Lanczos approach appears to be the best choice. © *2008 American Institute of Physics*. [DOI: 10.1063/1.2916581]

I. INTRODUCTION

Numerical simulation of the time-dependent Schrödinger equation (TDSE) is a tool of great importance for understanding, interpreting, and predicting the outcome of experimental studies of molecular systems. A theoretical description of experiments where the quantum system interacts with time-dependent fields, e.g., photons, involves a Hamiltonian which explicitly depends on time. Simulations employing models of pump-probe experiments are widely used in the physical chemistry and quantum chemistry communities.[1] These computations provide time-resolved data for dynamic systems and other types of laser pulse interactions, e.g., designed for optimal control of chemical reactions.

For time-independent Hamiltonians, a number of accurate and efficient propagators have been developed and used for many years, see, e.g., Ref. 2. The same type of schemes has also been studied by the numerical analysis community, see, e.g., the summary in Ref. 3. For propagation involving explicitly time-dependent Hamiltonians (cf. Ref. 4 (Chaps. 7 and 11), and references therein, and Ref. 5), the situation is less clear. Here, a difficulty when constructing accurate and efficient simulation schemes is that the fast oscillations in the time-dependent fields apparently necessitate quite small time steps. A common multiscale modeling approach to circumvent this problem is to use the *rotating wave approximation* (RWA), where a transformation removes the fast oscillations and only the average effect of the field is retained. However, as we will show below, this approach fails in some cases to provide an accurate solution. Then, an efficient scheme that fully resolves the time dependence must be used. In such cases, short-step schemes should be applied. A common choice in chemical physics is to use the second-order accurate split-operator method.[6] For highly accurate computations, which is the scope of this paper, we show that schemes with higher order of accuracy are more efficient for precise computations. We are aiming for methods that are capable of tackling high-dimensional problems but exemplify the performance on one dimensional problems in this paper. We then review and compare high-order Runge-Kutta-type solvers with conservation properties as well as the short-iterative Lanczos method combined with high-order representations of the propagator matrix based on the Magnus expansion. Some of the methods presented have not been applied to problems in quantum dynamics before. For a standard class of problems in quantum dynamics, we also derive an efficient fourth-order Magnus-Lanczos scheme which is very competitive.

In the next section, we introduce the class of quantum dynamics problems studied, along with a representation of the propagator for time-dependent Hamiltonians based on the Magnus expansion. Section III presents an analysis of the accuracy of the rotating wave approximation and some experiments relating the theory to computational results. Section IV reviews suitable numerical propagators for problems with explicitly time-dependent Hamiltonians and presents the new versions of the schemes briefly described above. In Sec. V, we compare the performance of the methods using the Rb_2 diatom as a model problem. This system is of interest for studies of a range of fundamental problems, from wave-packet dynamics and photoassociation to quantum control and Bose-Einstein condensation. Finally, the results are summarized in Sec. VI.

a)Electronic mail: hans.karlsson@kvac.uu.se.

II. THE TIME-DEPENDENT SCHRÖDINGER EQUATION

The TDSE is given by

$$i\hbar\frac{\partial}{\partial t}\Psi(r,t) = \hat{H}(t)\Psi(r,t),$$
$$\Psi(r,0) = \Psi_0(r), \tag{1}$$

where the Hamiltonian operator $\hat{H}(t)$ describes the system and $\Psi(r,t)$ denotes the wave function. At time $t=0$, the system is described by the wave function $\Psi_0(r)$. The spatial boundary conditions depend on the type of problem being studied.

To solve the TDSE (1) for realistic problems in molecular physics or chemistry, discrete (finite-dimensional) approximations in both time and space must be used. By introducing a discretization in space, the TDSE is turned into a large system of ordinary differential equations,

$$i\hbar\frac{d}{dt}\psi(t) = H(t)\psi(t),$$
$$\psi(0) = \psi^{(0)}, \tag{2}$$

where $H(t)$ is the Hamiltonian matrix and the wave function is now represented by the vector $\psi(t)$.

In this paper, we focus on numerical methods for the time propagation and use a pseudospectral discretization for the kinetic energy operator. Matrix-vector multiplication and exponentiation of the corresponding differentiation matrix can normally be computed efficiently using fast Fourier transforms (FFT). For problems with more than one spatial dimension, the Hamiltonian matrix can be written as a sum of Kronecker product matrices, implying that pseudospectral schemes can easily and efficiently be applied in different directions. Since pseudospectral schemes are spectrally accurate, the numerical error from the spatial discretization effectively vanishes as long as a sufficient number of grid points is employed, and then the discretization error in the computation only stems from the time propagation scheme.

If the Hamiltonian does not depend on time, i.e., $H(t) \equiv H$, the evolution matrix $U(t_{n+1},t_n)$ taking the grid function vector at t_n to $t_{n+1}=t_n+\Delta t$ is given in closed form,

$$\psi^{(n+1)} = U(t_{n+1},t_n)\psi^{(n)},$$
$$U(t_{n+1},t_n) = U(\Delta t) = e^{-iH\Delta t/\hbar}. \tag{3}$$

If the Hamiltonian depends explicitly on time, the time-evolution operator cannot be cast in the form given by Eq. (3). Instead, a time-ordered time-dependent perturbation expansion can be used. A drawback with this approach is that if the expansion series is truncated, the resulting propagator is not necessarily unitary. An alternative approach, retaining unitary propagation, is given by employing the *Magnus expansion*.[7,8] Assuming that Δt is sufficiently small, we can write the propagator in the form

$$U(t_{n+1},t_n) = \exp\left(\sum_{k=1}^{\infty} A_k(t_{n+1},t_n)\right), \tag{4}$$

where the matrices A_k involve time averages over commutators of $H(t)$. The first two terms can be written as [cf. Ref. 4 (Chap. 9.3)]

$$A_1(t_{n+1},t_n) = -\frac{i}{\hbar}\int_{t_n}^{t_{n+1}} H(\tau_1)d\tau_1,$$
$$A_2(t_{n+1},t_n) = -\frac{1}{2}\left(\frac{i}{\hbar}\right)^2\int_{t_n}^{t_{n+1}}\int_{t_n}^{\tau_1}[H(\tau_1),H(\tau_2)]d\tau_2 d\tau_1.$$

Note that A_k is of order $(\Delta t)^{2k-1}$, implying that truncating the Magnus series after the kth term yields an approximation to the evolution matrix of order $2k+1$.

We are interested in molecular systems where time-dependent fields, e.g., laser pulses, couple different electronic states. In addition to the time-dependent coupling, there might be static spin-orbit couplings or couplings caused by a breakdown of the Born-Oppenheimer approximation (Ref. 4, Sec. 12.1). For example, the Hamiltonian matrix for two coupled states is given by

$$H = \begin{pmatrix} T+V_g(r) & V_c(r,t) \\ V_c(r,t) & T+V_e(r) \end{pmatrix}, \tag{5}$$

and analogously for more coupled states. Here, T is the kinetic energy matrix and $V_{g/e}$ are diagonal matrices given by the ground/excited state potential functions. The coupling is described by the diagonal matrix $V_c(r,t)$.

III. ROTATING WAVE APPROXIMATION

As a model problem, consider a two-state system (5) with a coupling term $V_c(r,t)=V_c(t)$, representing a laser pulse of the form

$$V_c(t) = f(t)\cos(\omega t),$$

where we have a highly oscillatory term $\cos(\omega t)$ and a slowly varying envelope function $f(t)$. To solve the corresponding propagation problem numerically, the time step has to be quite small. A common approach to circumvent this is to use a multiscale modeling approach known as the RWA:[9] First, the wave function is transformed according to $\phi = W^{-1}\psi$, where

$$W = \begin{pmatrix} I & 0 \\ 0 & e^{-i\omega t}\cdot I \end{pmatrix},$$

and I is the unit matrix. This yields the following transformed TDSE,

$$i\hbar\frac{\partial\phi}{\partial t} = \begin{pmatrix} T+V_g & f(t)\cos(\omega t)e^{-i\omega t} \\ f(t)\cos(\omega t)e^{i\omega t} & T+V_e-\hbar\omega \end{pmatrix}\phi.$$

The time-dependent coupling can now be written as $\cos(\omega t)e^{\pm i\omega t}=\frac{1}{2}(1+e^{\pm i2\omega t})$. In the RWA, the highly oscillatory terms $e^{\pm i2\omega t}$ are neglected. The RWA Hamiltonian is then given by

$$H_{\mathrm{RWA}} = \begin{pmatrix} T + V_g & \frac{1}{2}f(t) \\ \frac{1}{2}f(t) & T + V_e - \hbar\omega \end{pmatrix}.$$

Note that the RWA transformation depends on the frequency of the pulse. If a second pulse of different frequency is introduced, the transformation has to be readjusted, and when several different pulses overlap, a simple transformation generally fails to model both pulses without any oscillatory term.

A. Theoretical analysis of the RWA

We now study the accuracy of the RWA: An analytic estimate of the error will be derived using the Magnus series representation of the propagator. Note that we use the Magnus expansion as an analytical tool and not as a basis for a numerical propagator. Hence, the error discussed in the following originates from the RWA modeling only. When propagating using H_{RWA} and any numerical integrator, an additional time-discretization error will be introduced.

Let

$$A_{\mathrm{RWA}}(t_{n+1},t_n) = -\frac{i}{\hbar}\int_{t_n}^{t_{n+1}} H_{\mathrm{RWA}}(\tau)d\tau$$

denote the first Magnus term for the RWA Hamiltonian. Correspondingly, denote the first term in the neglected part of the true Hamiltonian by

$$A_{\omega}(t_{n+1},t_n) = -\frac{i}{\hbar}\int_{t_n}^{t_{n+1}} \times \begin{pmatrix} 0 & [f(\tau)/2]e^{-i2\omega\tau}\cdot I \\ [f(\tau)/2]e^{i2\omega\tau}\cdot I & 0 \end{pmatrix} d\tau. \tag{6}$$

Then, for sufficiently small Δt, we have that

$$\phi^{(n+1)} = e^{A^n_{\mathrm{RWA}}+A^n_{\omega}}\phi^{(n)} + \mathcal{O}((\Delta t)^3),$$

where $A^n_{\mathrm{RWA}/\omega} = A_{\mathrm{RWA}/\omega}(t_{n+1},t_n)$ denote the operators in the $(n+1)$th time interval $[t_n,t_{n+1}]$. Hence, at a final time after N Δt intervals, we have

$$\phi^{(N)} = \prod_{n=0}^{N-1} e^{A^n_{\mathrm{RWA}}+A^n_{\omega}}\phi^{(0)} + \mathcal{O}((\Delta t)^2). \tag{7}$$

Note that $A^n_{\mathrm{RWA}} = \mathcal{O}(\Delta t)$ and $A^n_{\omega} = \mathcal{O}(\Delta t)$. Using the Baker-Campbell-Hausdorff formula,[10] this yields

$$e^{(A^n_{\mathrm{RWA}}+A^n_{\omega})} = e^{(A^n_{\omega}+(1/2)[A^n_{\mathrm{RWA}},A^n_{\omega}])}e^{(A_{\mathrm{RWA}})} + \mathcal{O}((\Delta t)^3).$$

Let $B^n = A^n_{\omega} + \frac{1}{2}[A^n_{\mathrm{RWA}},A^n_{\omega}]$. We can then reformulate Eq. (7) to

$$\phi^{(N)} = \prod_{n=0}^{N-1} e^{B^n}e^{A^n_{\mathrm{RWA}}}\phi_0(t_0) + \mathcal{O}((\Delta t)^2).$$

Quantitatively, it is easy to argue that the RWA can be useful. Performing the integration of the neglected terms in Eq. (6) over one period of the fast oscillation gives a relatively small result, and the size depends on the variation of the envelope function over the period. Since the envelope is first growing and then decreasing, the different terms A^n_{ω} also cancel when summing over the whole time interval where the envelope function has a significant nonzero value.

We now discuss the error in more detail and derive formulas that can be used for a quantitative description of it. The period of the oscillating term is given by π/ω. If this quantity is sufficiently small and the derivative of $f(t)$ is bounded independently of ω and t (as usually is the case), it holds for an arbitrary choice of t that

$$\left|\int_t^{t+\pi/\omega} f(\tau)e^{\pm 2i\omega\tau}d\tau\right| = \left|\int_t^{t+\pi/\omega} (f(\tau)-\bar{f})e^{\pm 2i\omega\tau}d\tau\right|$$
$$\leq \|f-\bar{f}\|_{L_\infty}\cdot\frac{\pi}{\omega} \leq \left\|f'\cdot\frac{\pi}{\omega}\right\|_{L_\infty}\cdot\frac{\pi}{\omega}$$
$$= \mathcal{O}\left(\left(\frac{\pi}{\omega}\right)^2\right),$$

where $\bar{f} = [1/(\pi/\omega)]\int_t^{t+\pi/\omega} f(\tau)d\tau$ denotes the mean value of f in the interval. The next to last step is due to the mean value theorem. In particular, this assures that $\Sigma_{n=l_1}^{l_m} A^n_{\omega} = \mathcal{O}(\Delta t + (\pi/\omega)^2\cdot(t_{l_m}-t_{l_1}))$ and thus, by expansion of the exponential function,

$$\prod_{n=l_1}^{l_m} e^{A^n_{\omega}} = I + \sum_{n=l_1}^{l_m} A^n_{\omega} + \mathcal{O}\left(\left(\Delta t + \left(\frac{\pi}{\omega}\right)^2\cdot(t_{l_1}-t_{l_m})\right)^2\right). \tag{8}$$

Based on these considerations, we can estimate the ℓ_2 error induced by the RWA as follows:

$$\phi^{(N)} - \phi^{(N)}_{\mathrm{RWA}} = -\phi^{(N)}_{\mathrm{RWA}} + \prod_{n=0}^{N-1} e^{A^n_{\mathrm{RWA}}+A^n_{\omega}}\phi^{(0)} + \mathcal{O}((\Delta t)^2)$$
$$= -\phi^{(N)}_{\mathrm{RWA}} + \left(\prod_{n=0}^{N-1} e^{B^n}\cdot\prod_{n=0}^{N-1} e^{A^n_{\mathrm{RWA}}}\right)\phi^{(0)} + \mathcal{O}((\Delta t)^2) + \sum_{n=0}^{N-2}\prod_{l=0}^{n-1}(e^{B^l}e^{A^l_{\mathrm{RWA}}})e^{B^n}\left[e^{A^n_{\mathrm{RWA}}}, \prod_{l=n+1}^{N-1} e^{B^l}\right]\prod_{l=n}^{N-1} e^{A^l_{\mathrm{RWA}}}$$
$$= \sum_{n=0}^{N-1}\left(A^n_{\omega} + \frac{1}{2}[A^n_{\mathrm{RWA}},A^n_{\omega}]\right)\phi^{(N)}_{\mathrm{RWA}} + \sum_{n=0}^{N-2}\prod_{l=0}^{n-1}(e^{B^l}e^{A^l_{\mathrm{RWA}}})e^{B^n}\left[e^{A^n_{\mathrm{RWA}}}, \prod_{l=n+1}^{N-1} e^{B^l}\right]\prod_{l=n}^{N-1} e^{A^l_{\mathrm{RWA}}}\phi^{(0)}$$
$$+ \mathcal{O}\left(\left(\Delta t + \left(\frac{\pi}{\omega}\right)^2\cdot t_N\right)^2\right),$$

where we used Eq. (8) in the last step.

The second term is difficult to handle since the commutator is evaluated at different times. However, we may proceed by studying the norm of the error,

$$\begin{aligned}\|\phi^{(N)}-\phi^{(N)}_{\mathrm{RWA}}\|_2 &= \left\|\sum_{n=0}^{N-1}\left(A^n_\omega+\frac{1}{2}[A^n_{\mathrm{RWA}},A^n_\omega]\right)\right\|_2\|\phi^{(N)}_{\mathrm{RWA}}\|_2+\sum_{n=0}^{N-2}\left\|\prod_{l=0}^{n-1}(e^{B^l}e^{A^l_{\mathrm{RWA}}})e^{B^n}\right\|_2\Bigg\|\\ &\times\left[e^{A^n_{\mathrm{RWA}}},\prod_{l=n+1}^{N-1}e^{B^l}\right]\Bigg\|_2\left\|\prod_{l=n}^{N-1}e^{A^l_{\mathrm{RWA}}}\phi^{(0)}\right\|_2+\mathcal{O}\left(\left(\Delta t+\left(\frac{\pi}{\omega}\right)^2\cdot t_N\right)^2\right)\\ &\leqslant\left\|\sum_{n=0}^{N-1}\left(A^n_\omega+\frac{1}{2}[A^n_{\mathrm{RWA}},A^n_\omega]\right)\right\|_2+\sum_{n=0}^{N-2}\left\|\left[e^{A^n_{\mathrm{RWA}}},\prod_{l=n+1}^{N-1}e^{B^l}\right]\right\|_2+\mathcal{O}\left(\left(\Delta t+\left(\frac{\pi}{\omega}\right)^2\cdot t_N\right)^2\right).\end{aligned}\tag{9}$$

It remains to compute the commutators $[A^n_{\mathrm{RWA}},A^n_\omega]$ and $[e^{A^n_{\mathrm{RWA}}},\Pi_{l=n+1}^{N-1}e^{B^l}]$. For this purpose, we introduce the notations $\Delta V\equiv V_e-\hbar\omega-V_g$, $g_n\equiv\int_{t_n}^{t_{n+1}}f(\tau)d\tau$, $h_k\equiv\int_{t_{n+1}}^{t_N}f(\tau)\cdot e^{-2i\omega}d\tau$, and

$$r_n\equiv\Sigma_{l=n+1}^{N-1}g_k\cdot\int_{t_n}^{t_{n+1}}f(\tau)\cdot(e^{2i\omega\tau}-e^{-2i\omega\tau})d\tau.$$

For the first commutator, we sum up over the time steps yielding

$$\sum_{n=0}^{N-1}\frac{1}{2}[A^n_{\mathrm{RWA}},A^n_\omega]=\frac{1}{2\hbar^2}\begin{pmatrix}r_{-1}\cdot I & -h_{-1}\Delta V\\ h^*_{-1}\Delta V & -r_{-1}\cdot I\end{pmatrix}.\tag{10}$$

Using Eq. (10) on the interval $[t_{k+1},t_N]$ and estimate (8), we rewrite the second commutator as

$$\begin{aligned}\left[e^{A^n_{\mathrm{RWA}}},\prod_{l=n+1}^{N-1}e^{B^l}\right] &= \left[I+A^n_{\mathrm{RWA}}+\mathcal{O}((\Delta t)^2),I+\sum_{l=n+1}^{N-1}B^l+\mathcal{O}\left(\left(\Delta t+\left(\frac{\pi}{\omega}\right)^2\cdot(t_N-t_{n+1})\right)^2\right)\right]\\ &=\left[A^k_{\mathrm{RWA}},\sum_{l=k+1}^{N-1}\left(A^l_\omega+\frac{1}{2}[A^l_{\mathrm{RWA}},A^l_\omega]\right)\right]+\mathcal{O}\left(\left(\Delta t+\left(\frac{\pi}{\omega}\right)^2\cdot(t_N-t_{n+1})\right)^2\cdot\Delta t\right)\\ &=\frac{1}{2\hbar^2}\begin{pmatrix}g_n(h^*_n-h_n)\cdot I & -h_n\Delta V\\ h^*_n\Delta V & g_n(h_n-h^*_n)\cdot I\end{pmatrix}\\ &\quad-\frac{i}{2\hbar^3}\begin{pmatrix}g_n(h^*_n+h_n)\Delta V & -h_n((\Delta V)^2+[T,\Delta V])+2r_n\cdot g_n\cdot I\\ h^*_n((\Delta V)^2+[T,\Delta V])-2r_n\cdot g_n\cdot I & -g_n(h^*_n+h_n)\Delta V\end{pmatrix}\\ &\quad+\mathcal{O}\left(\left(\Delta t+\left(\frac{\pi}{\omega}\right)^2\cdot(t_N-t_{n+1})\right)^2\cdot\Delta t\right).\end{aligned}$$

Finally, the ℓ_2 norm of the commutator can be estimated by computing its infinity norm.

From the formulas above, we see that combinations of the terms g_k and h_k govern the error. Our first observation is that the error depends on the variation of the envelope function f over a period π/ω of the fast oscillation. Furthermore, a scaling of $f(t)$ has a linear effect on the terms g_i and h_i. Hence, to first order, the error increases linearly in the pulse intensity. For pulses that are strong compared to ΔV, the error increases even quadratically in the intensity. Also, the length of the support of the envelope function affects the size of the error. For an envelope function of the form $f(t)=(1/\sqrt{2\pi}\sigma)e^{-(1/2)[(t-t_0)/\sigma]^2}$, i.e., a normalized Gaussian, the error term does not depend on σ. To sum up, the error is growing with decreasing frequency ω of the oscillation and, with increasing scaling, slope as well as width of the envelope function.

We also note that the RWA introduces an averaging of the effects over one period of the fast oscillation. Therefore, it fails to resolve the effects on this smaller scale, and it is natural that the RWA error cannot be reduced further by using a time step smaller than π/ω. On this scale, the contribution of A_ω is no longer small compared to A_{RWA}. Hence, the solution computed based on H_{RWA} will not converge to the exact solution as the time step is reduced: A systematic error takes over when Δt is reduced below π/ω.

B. An experiment illustrating the error induced by the RWA

In the previous section, we presented a theoretical analysis of the accuracy of the RWA modeling approach. We now also demonstrate the accuracy of the RWA by performing numerical experiments for the two-state system presented in Sec. V. We use $V_c(t)=E_0\cdot e^{(-(1/2)[(t-t_0)/\sigma]^2)}\cos(\omega(t-t_0))$, where $E_0=21.9$ cm^{-1}, and compare the solutions for the true Hamiltonian and the one obtained by the RWA modeling. For the propagation, we use the fourth-order Magnus-Lanczos scheme later described in Sec. IV B 3. Figure 1(b) shows the relative error in the population of the excited state and Fig. 1(a) the relative error in the overlap with the initial state $\psi_0(x)$, i.e., the cross-correlation function

$$C(t_N)=\int \psi_0^*(x)\psi(x,t_N)dx. \tag{11}$$

From Fig. 1, we see that when using the RWA, the relative error in the population cannot be reduced below 1.5%, and the relative error in the cross-correlation function flattens out at 0.33%.

Another conclusion from Fig. 1 is that if low accuracy is sufficient and a correspondingly large time step is used, propagation using H_{RWA} can yield better results than if the true Hamiltonian is used. This is not a surprise, since for such large time steps, the oscillations are not resolved in the propagation using the full coupling term, resulting in a large numerical error. To get a highly accurate solution, the true Hamiltonian matrix $H(t)$ must be employed and the fast oscillations must be fully resolved.

We now estimate the error for the problem described above using the formulas from the theoretical analysis in the previous section. First, note that $\int_{t_0}^{t_N} f(\tau)e^{-2i\omega\tau}d\tau\approx -1.7\times 10^{-6}$ and

$$\frac{1}{2}\sum_{n=0}^{N-1}[A_{\mathrm{RWA}}^n,A_\omega^n]\approx\begin{pmatrix}-i\cdot 7.9\times 10^{-12}\cdot I & -8.4\times 10^{-7}\Delta V\\ 8.4\times 10^{-7}\Delta V & i\cdot 7.9\times 10^{-12}\cdot I\end{pmatrix}.$$

The first error term in Eq. (9) is thus comparatively small. For the second commutator, we compute the absolute sum of the different terms separately, yielding

$$\frac{1}{2\hbar^2}\sum_{n=0}^{N-1}\begin{pmatrix}|g_n(h_n^*-h_n)|\cdot I & |h_n\Delta V|\\ |h_n^*\Delta V| & |g_n(h_n-h_n^*)|\cdot I\end{pmatrix}\approx\begin{pmatrix}0.011\cdot I & 1.0|\Delta V|\\ 1.0|\Delta V| & 0.011\cdot I\end{pmatrix} \tag{12}$$

and

$$\frac{1}{2\hbar^3}\sum_{n=0}^{N-1}\begin{pmatrix}|g_n(h_n^*+h_n)\Delta V| & |h_n((\Delta V)^2+[T,\Delta V])|+|2r_n\cdot g_n|\cdot I\\ |h_n^*((\Delta V)^2+[T,\Delta V])|+|2r_n\cdot g_n|\cdot I & |g_n(h_n^*+h_n)\Delta V|\end{pmatrix}\approx\begin{pmatrix}0.0054|\Delta V| & 0.51|(\Delta V)^2+[T,\Delta V]|+1.0\times 10^{-7}\\ 0.51|(\Delta V)^2+[T,\Delta V]|+1.0\times 10^{-7} & 0.0054|\Delta V|\end{pmatrix}.$$

Since $\max_x\Delta V(x)\approx 9.5\times 10^{-3}$, the error is dominated by the matrix (12). Its maximum norm is $0.011+1.0\max|\Delta V|\approx 0.021$.

This is an estimate for the error in the ℓ_2 norm, but it serves as a good guess for the error in other functionals of the solution (depending, of course, on the portion of the error in the direction of this functional) as the results of our experiment show. Hence, the analysis presented above can be useful in practice.

IV. PROPAGATORS

As remarked in the previous section, an accurate and efficient propagator for the original problem is needed if we want to include the effect of, e.g., a high oscillatory coupling term for a problem where the error using the RWA approximation is not acceptable. We will discuss two approaches for constructing such propagators: viewing Eq. (2) as a classical Hamiltonian system and using partitioned Runge-Kutta methods and employing an exponential integrator in combination with the Magnus series representation (4) of the propagator. A third alternative is to use the so called (t,t') method[11] which adds the "time" t' as an additional space dimension and thereby rephrases the problem as an autonomous system where Eq. (3) can be applied. This, however, increases the memory consumption considerably which will be a problem in higher dimensional settings.

When comparing the computational complexity for different methods, we focus on the number of FFT/IFFT pairs performed by the time-propagation scheme, since this part of the work dominates the computational cost for all of the propagators used.

A. Geometric numerical integration

Considering Eq. (2) as a system of ordinary differential equations, we may apply standard one-step methods, e.g., Runge-Kutta-type integrators. This is a wide class of schemes, and we restrict the discussion to methods that preserve the basic unitarity structure of the exact evolution operator.

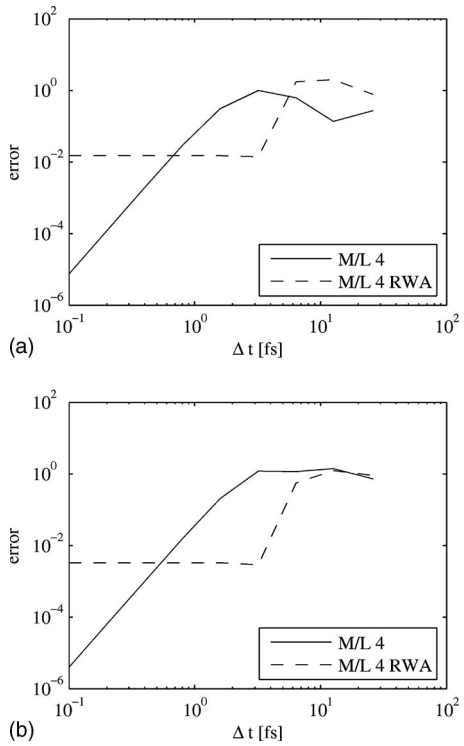

FIG. 1. Comparison of the results with and without the RWA. (a) Relative error in the cross-correlation function. (b) Relative error in the population of PES 2.

We follow Gray and Verosky[12] and rearrange the system: Consider a time-independent, real Hamiltonian matrix H and split the wave function vector ψ into its real and imaginary parts. This yields a classical Hamiltonian system. Gray and Verosky point out that area preservation of the flow for the classical Hamiltonian system assures norm conservation in the quantum system (cf. also Ref. 13). For classical Hamiltonian systems, symplectic numerical integrators preserve the area of the flow. Explicit, symplectic schemes for separable Hamiltonian systems can be found among the class of *partitioned Runge-Kutta (PRK) methods*. If the Hamiltonian matrix is time independent, it is indeed separable into two parts, e.g., one only depending on the real and one only on the imaginary part of the wave function. Sanz-Serna and Portillo[5] broaden this ansatz to explicitly time-dependent Hamiltonians by transforming the system into an autonomous equation by introducing an additional conjugate pair of variables $(\mathcal{P},\mathcal{T}=t)$.

The explicit PRK schemes for the generalized coordinates Q and generalized momenta P, i.e., in our case the real and imaginary parts of the wave function vector, are given by (cf. Ref. 5)

$$Q_{n,i} = Q_{n,i-1} + \Delta t \frac{B_i}{\hbar} H(t_n + c(i)\Delta t) P_{n,i}, \quad i = 1, \ldots s,$$

$$P_{n,i} = P_{n,i-1} + \Delta t \frac{b_i}{\hbar} H(t_n + C(i)\Delta t) Q_{n,i}, \quad i = 1, \ldots s, \quad (13)$$

where $c_i = \Sigma_{j=1}^{i-1} b_j$ and $C_i = \Sigma_{j=1}^{i} B_j$. Note that this type of scheme is very memory efficient. Only two real vectors, one for Q and one for P (equivalent to a single complex wave function vector), are required. A particular method of type (13) is specified by the number of stages s and the sets of weights b and B. To achieve a certain order of accuracy, the weights have to satisfy certain order conditions, and to assure that the scheme is symplectic, additional conditions need to be fulfilled, see, e.g., Ref. 14. If the number of stages is large enough, the parameters can also be adjusted such that, e.g., the error constant is minimal or the stability domain is maximal.

In our numerical experiments presented in the next section, we use a fourth-order method with seven stages and a sixth-order scheme with 11 stages, both derived in Ref. 15 by optimizing the efficiency of the symplectic PRK method given a certain accuracy. For the problems that we study, which include explicit time dependence, we have found these methods to be more efficient than the methods described in Refs. 16 and 17, proposed for the TDSE with time-independent Hamiltonians, as well as the minimal error constant method proposed in Ref. 18.

Complexity. In general, an s step partitioned Runge-Kutta method involves $2s$ multiplications of the Hamiltonian with a (real) vector, i.e., to the leading order $2s$ real FFT/IFFT pairs. The methods proposed above have 7 and 11 stages. However, since they possess the first-same-as-last property, only 12 or 20 real FFT/IFFT pairs are needed. We do not only save the last step for the imaginary part (since $b_s = 0$) but can also combine the last step for the real part with the first step for the new time interval.

B. Exponential integrators

Designing a numerical method based on form (4) of the evolution operator involves primarily two aspects: a suitable truncation of the Magnus series expansion and an efficient scheme for computing the matrix exponential. Numerically, to evolve the current wave function vector $\psi^{(n)}$ to $\psi^{(n+1)}$, we need to compute the matrix-vector multiplication $e^{-(i/\hbar)\bar{H}\Delta t}\psi^{(n)}$, where $\bar{H}$ denotes some averaged version of the Hamiltonian based on the Magnus expansion. Below, we discuss some interesting choices. For a short overview of exponential integrators, see Ref. 3.

1. The split-operator method

The idea behind the split-operator methods[19,20] is to compute the matrix exponential by *splitting* the Hamiltonian matrix into parts corresponding to kinetic and potential energy,

$$e^{-i\bar{H}\Delta t/\hbar} = e^{-iT\Delta t/(2\hbar)} e^{-i\bar{V}\Delta t/\hbar} e^{-iT\Delta t/2\hbar} + \mathcal{O}((\Delta t)^3), \quad (14)$$

where we have assumed that only the potential energy matrix is time-dependent and needs to be averaged. This scheme is commonly used in chemical physics, especially for problems when there is an easily computable diagonal representation of the kinetic energy matrix. Note that the splitting (14) is second-order accurate, and it is reasonable to truncate the Magnus expansion after the first term. This simply corresponds to evaluating the potential energy at the midpoint of the time interval.

Higher order accurate splitting schemes can also be derived, see e.g. Refs. 21–23 In fact, there is a close relationship between splitting methods and PRK schemes, see e.g. Refs. 18 and 24

Complexity. For the split-operator method, one (complex) FFT/IFFT pair is needed for each $e^{-iT\Delta t/(2\hbar)}$-term. However, this scheme again has the first-same-as-last property, i.e. we can combine the last kinetic energy term with the first one of the next step. Hence, in effect one complex FFT/IFFT is required per time step.

2. The short-iterative Lanczos scheme

An alternative method for calculating the matrix exponential applied to a vector is to use a polynomial expansion. In the Lanczos process,[25] (Ref. 26 Chap. 7), a polynomial expansion is recursively created that builds an orthonormal basis in the pth order Krylov subspace spanned by $\{\psi^{(n)},\bar{H}\psi^{(n)},\bar{H}^2\psi^{(n)},\ldots,\bar{H}^{p-1}\psi^{(n)}\}$. The approximate solution is then given by the projection of the exact solution to the Krylov subspace. In chemical physics, the term *short-iterative Lanczos (SIL) propagator* usually refers to the version of this scheme were the Hamiltonian is evaluated at the midpoint of the time interval, resulting in second-order accuracy.

In the Lanczos scheme, we need to chose p, i.e., the size of the Krylov subspace. Note that, for a time-independent Hamiltonian matrix, there is a relation between the p stage Lanczos scheme and a $(p-1)$th stage PRK method. In both cases, the propagated solution lies in the pth order Krylov space. One difference is that the coefficients in the linear combination of the basis vectors are fixed for the PRK method, whereas they are dynamically determined in the Lanczos algorithm. If the Hamiltonian is time dependent, the situation is somewhat different. Then the time where $H(t)$ is evaluated changes in the different stages in the PRK algorithm, while in the Lanczos method we are using the same averaged matrix $\bar{H}$ in all stages.

Using a larger p in the Lanczos method might allow for a longer time step (a larger p, in a sense, corresponds to increasing the order of accuracy of the scheme). However, larger values of p can also induce loss of orthogonality in the orthogonal basis, resulting in numerical problems. For problems with an explicitly time-dependent potential, the argument in Sec. III shows that the time step should be chosen relatively small, resulting in that a moderately large Krylov subspace can be used. In the experiments in Sec. V, we use $p=5$ which yields good results for the time steps considered. If one wants to determine p dynamically (corresponding to a p-adaptive scheme), Hochbruck *et al.*[27] propose to stop the Lanczos iterations as soon as the generalized residual is small enough, i.e.,

$$\Delta t|e^{-i/\hbar\Delta t J_p}|_{p,1}(J_{p+1})_{p+1,p} < \mathrm{tol},$$

where J_p is the approximation of the matrix $\bar{H}$ in the p-dimensional Krylov space.

Complexity. The Lanczos method involves one multiplication of the Hamiltonian matrix with a vector in each iteration, i.e., p (complex) FFT/IFFT pairs are required per time step, neglecting the work for solving the small eigenvalue problem for J_p.

3. The Magnus-Lanczos method

When the Lanczos algorithm is used for time propagation, its asymptotic converge rate in p is superlinear.[27] The performance can be compared to spectral methods, i.e., after a certain number of Lanczos stages, the time-discretization error decreases very rapidly. The properties of the Hamiltonian matrix and the time step determine from which stage this occurs. For time-dependent Hamiltonian matrices, the error induced by using the first term in the Magnus expansion may dominate already for relatively small time steps. In such cases, the step size can be enlarged by including higher order terms from the Magnus expansion. However, these terms involve an increasing number of commutators, making the computations more and more costly. A comparison of the first- and second-order Magnus truncation is given by Tal-Ezer *et al.*[28] Blanes *et al.*[29] propose the following fourth-order truncation of the Magnus expansion, designed to reduce the number of commutators,

$$A_1(t_{n+1},t_n) = \Delta t B^{[0]}, \quad A_2(t_{n+1},t_n) = -(\Delta t)^2[B^{[0]},B^{[1]}],$$

where

$$B^{[k]} = \frac{1}{(\Delta t)^{k+1}}\int_{-\Delta t/2}^{\Delta t/2} \tau^k \frac{-i}{\hbar} H\left(t_n + \frac{\Delta t}{2} + \tau\right) d\tau.$$

We now note that, for specific problem classes, the terms in these formulas can be further simplified so that commutators need not be computed. We derive a simple form of the two first terms of the Magnus expansions for the case of a nuclear Hamiltonian for the coupling of different electronic states, where each coupling is either time or space dependent. As an example, we study the following three-state system:

$$H = \begin{pmatrix} T+V_g(r) & V_1(t) & 0 \\ V_1(t) & T+V_{e1}(r) & V_2(r) \\ 0 & V_2(r) & V_{e2}(r) \end{pmatrix}, \tag{15}$$

where we have three potential energy surfaces $V_{g/e1/e2}$, a dynamic coupling term $V_1(t)$, and a static coupling term $V_2(r)$ (cf. Ref. 30 for an application of a system of this type). Note that, in the Condon approximation, a dynamical coupling term is considered to be space independent.

For example (15), the commutators can be computed analytically and the matrix $\bar{H}$ is defined by

$$A_1(t_{n+1},t_n) = -\frac{i}{\hbar}\cdot\Delta t\cdot\begin{pmatrix} T+V_g & C_0 & 0 \\ C_0 & T+V_{e1} & V_2 \\ 0 & V_2 & T+V_{e2} \end{pmatrix},$$

$$A_2(t_{n+1},t_n) = \frac{1}{\hbar}\cdot(\Delta t)^2\cdot C_1\cdot\begin{pmatrix} 0 & -(V_{e1}-V_g) & -V_2 \\ (V_{e1}-V_g) & 0 & 0 \\ V_2 & 0 & 0 \end{pmatrix},$$

where

$$C_0 = \frac{1}{\Delta t} \cdot \int_{-\Delta t/2}^{\Delta t/2} V_1\left(t_n + \frac{\Delta t}{2} + \tau\right) d\tau$$

$$C_1 = \frac{1}{(\Delta t)^2} \cdot \int_{-\Delta t/2}^{\Delta t/2} V_1\left(t_n + \frac{\Delta t}{2} + \tau\right) \cdot \tau d\tau.$$

The integrals $C_{0,1}$ can either be evaluated analytically or using numerical integration. In the latter case, the formula has to be at least fourth-order accurate for C_0 and second-order accurate for C_1 in order to assure fourth-order accuracy of the resulting scheme. In this case, the shape of the second Magnus term is appealing, since no kinetic energy term is involved. Including the second term leads to a fourth-order accurate propagator whose performance ameliorates the classical SIL propagator at little extra cost.

However, higher order Magnus terms are unfortunately still very complicated. They involve commutators of kinetic and potential energies and are thus more expensive to evaluate. This can be seen already considering the following two-state system:

$$H = \begin{pmatrix} T + V_g(r) & V(t) \\ V(t) & T + V_e(r) \end{pmatrix}.$$

For a sixth-order accurate approximation of the propagator, the following three additional terms are needed:

$$\begin{aligned} A_3(t_{n+1}, t_n) &= -i\frac{6}{5} C_1^2 (\Delta t)^3 \begin{pmatrix} \Delta V & 0 \\ 0 & \Delta V \end{pmatrix} - i\frac{1}{2}\left(C_2 - \frac{C_0}{12}\right)(\Delta t)^3 \begin{pmatrix} -2C_0\Delta V & -(\Delta V)^2 + [T,\Delta V] \\ -(\Delta V)^2 - [T,\Delta V] & 2C_0\Delta V \end{pmatrix} \\ &\quad - \frac{1}{60} C_1 (\Delta t)^4 \begin{pmatrix} -4C_0[T,\Delta V] & 4C_0^2\Delta V + (\Delta V)^3 + [T,[T,\Delta V] - (\Delta V)^2] + V_a[T,\Delta V] - [T,\Delta V]V_b \\ -4C_0^2\Delta V - (\Delta V)^3 - [T,[T,\Delta V] + (\Delta V)^2] - V_b[T,\Delta V] + [T,\Delta V] & 4C_0[T,\Delta V] \end{pmatrix}, \end{aligned}$$

where $\Delta V = V_e - V_g$ and

$$C_2 = \frac{1}{(\Delta t)^3} \cdot \int_{-\Delta t/2}^{\Delta t/2} f\left(t_n + \frac{\Delta t}{2} + \tau\right) \cdot \tau^2 d\tau.$$

When applying the kinetic energy matrix using FFT/IFFT, we have to expand all the commutators in these formulas. This means that we have to compute the four first spatial derivative of $\psi^{(n)}$ in each step, i.e., four FFT/IFFT pairs compared to only one for the fourth-order scheme. The corresponding time-propagation algorithm is not competitive even if the error constant is rather small. However, note that some terms in the third Magnus term A_3 can be further simplified when using a sparse matrix representation of the kinetic energy instead of using FFT/IFFT. Hence, the performance of the sixth-order Magnus-Lanczos method is presumably comparably better if a finite difference scheme is used for discretizing the kinetic energy operator instead of a pseudospectral scheme.

Above, we have derived a fourth-order Magnus expansion that is commutator-free for Hamiltonians with either time- or space-independent coupling terms. If some coupling term of the form $V_c(r,t)$ is involved, already the second Magnus term contains commutators and at least one additional FFT/IFFT pair is needed to compute the first derivative of the wave function. Blanes and Moan[31] propose commutator-free integrators for systems where time and spatial dependency can be factorized. They make, however, use of a splitting of the time step in mutiple substeps, and in each step several, for fourth-order accuracy, at least two matrix exponentials must be evaluated. A theoretical study of the shape of the Magnus expansion for a number of quantum Hamiltonians can be found in Ref. 32.

The derivation of the Magnus expansion requires a quite restrictive bound on the time step. However, using a truncated version of the Magnus expansion, larger step sizes still give good quality results, a fact that is explained in Ref. 33.

Complexity. In the Magnus-Lanczos schemes described above, one multiplication of the sum of the Magnus terms with a wave function is needed per Lanczos iteration. Since several terms of the Magnus expansion are involved, this becomes more costly than the standard Lanczos method. However, for our new commutator-free fourth-order Magnus-Lanczos method, the complexity is not increased (to leading order) compared to the standard second-order accurate SIL method.

V. NUMERICAL EXPERIMENTS

To compare the performance of the different time-propagation methods, we study the interaction of the Rb_2 diatom with a femtosecond laser pulse.

The spatial coordinate is discretized using the Fourier pseudospectral method on a grid with 256 points. The action of the kinetic energy matrix is computed using a FFT/IFFT pair, and the potential functions for the electronic states are taken from Park *et al.*[34] In the first set of experiments, two states are coupled via a fast laser pulse modeled by $V_c(t) = E_0 e^{-(1/2)[(t-t_0)/\sigma]^2} \cos(\omega(t-t_0))$, where the light-matter interaction is treated semiclassically and the Condon approximation is used, i.e., the transition dipole moment is assumed to

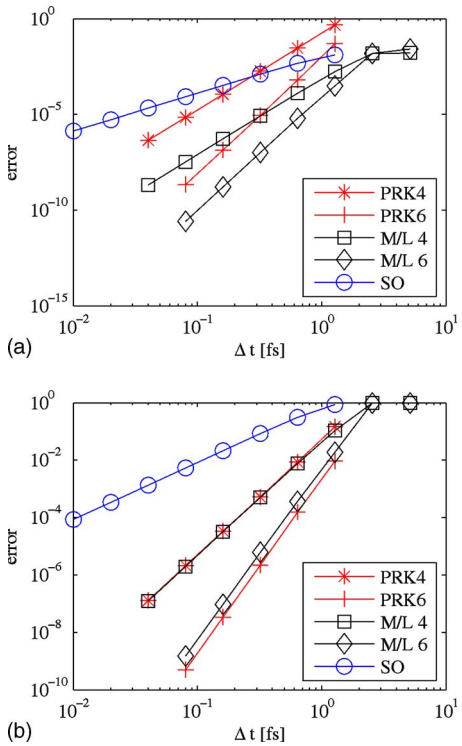

FIG. 2. (Color online) Accuracy of the different methods. (a) Cross-correlation function. (b) Population.

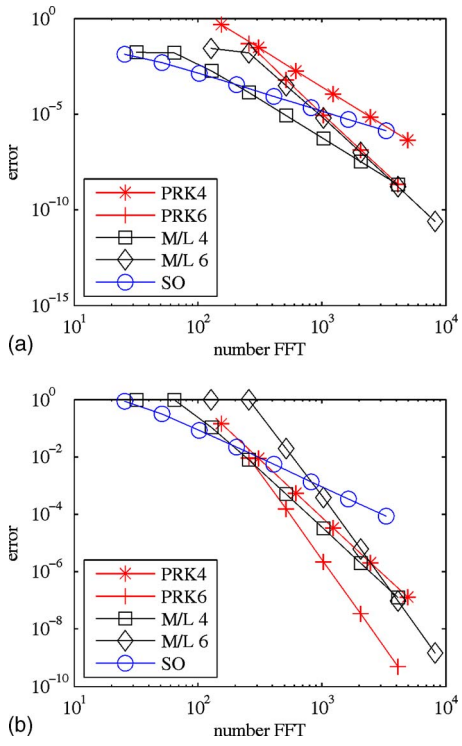

FIG. 3. (Color online) Efficiency of the different methods. (a) Cross-correlation function. (b) Population.

be constant. In the second set of experiments, a third state is added, coupled to the second state via a spin-orbit interaction.

We will compare the following numerical schemes: split-operator (SO), a fourth-order-seven-stage partitioned Runge-Kutta (PRK4) and a sixth-order-eleven-stage partitioned Runge-Kutta (PRK6)—both developed in Ref. 15—as well as the commutator-free fourth order Magnus-Lanczos propagator (M/L 4) and its sixth order extension (M/L 6).

A. Modeling a pump-pulse experiment

In our first test case, a pump-pulse couples the Rb_2 $X\ ^1\Sigma_g^+$ ground state with the $A\ ^1\Sigma_u^+$ excited state. We use a laser pulse length of 100 fs, the wavelength is $\lambda=1000$ nm (and thus $\omega\approx 1.9/\text{fs}$), and the strength of the pulse is set to $E_0=21.9\ \text{cm}^{-1}$. As a reference solution, we solved the TDSE with the M/L 4 method using a time step of $\Delta t=0.001$ fs.

Order of accuracy and efficiency. To compare the different methods, we compute the population in the excited state when the pulse is over as well as the cross correlation with the wave function and the lowest vibrational state in the ground state. Figure 2 shows the relative error (compared to the reference solution) in the population as well as in the cross-correlation function (11) as a function of the step size Δt.

As predicted, the PRK4 and M/L 4 methods show fourth-order, the PRK6 and the M/L 6 show sixth-order, and the SO method shows second-order accuracy. The error constants are smaller for the M/L methods than for the PRK methods of the same order at least for the cross-correlation function.

In Fig. 3, work (in terms of the number of real FFT/IFFT's involved) of the different methods is related to the error. The graph for the cross-correlation function shows that for very low accuracy requirements, the SO method performs best, for more accurate computations the M/L 4 algorithm, and for extremely high accuracy the PRK6 method. The regions where the different methods are most effective depend, of course, on the problem parameters.

From Fig. 3, we also note that in the case of the population, where only the absolute value and not any phase information is needed, the PRK methods are comparable in their quality to the M/L methods.

Note that the stability domain of the PRK methods allows for relatively large time steps such that it is possible to do low-accuracy computations with the chosen PRK methods.

Unitarity. Since the probability density of the nuclei, $\int_{\mathbb{R}}|\psi(r,t)|^2 dr$, is conserved, a good numerical method should preserve this property as well. In Table I, the largest deviation from one under calculations with different values of Δt is shown.

Table I shows that the norm is conserved for M/L and

TABLE I. Norm conservation. Largest deviation from unity during the computation with time step Δt up to $t=340$ fs.

	$\Delta t=0.16$ fs	$\Delta t=0.32$ fs	$\Delta t=0.64$ fs
PRK4	1.7×10^{-6}	2.7×10^{-5}	4.9×10^{-4}
PRK6	5.0×10^{-9}	3.3×10^{-7}	2.6×10^{-5}
M/L 4	2.7×10^{-15}	2.7×10^{-15}	3.2×10^{-15}
M/L 6	2.8×10^{-15}	3.1×10^{-15}	2.7×10^{-15}
SO	2.4×10^{-13}	1.1×10^{-13}	5.9×10^{-14}

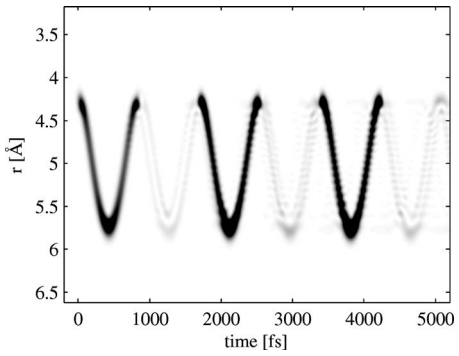

FIG. 4. Probability distribution for the $A\ ^1\Sigma_u^+$ state.

SO, up to the order where round-off errors appear. For both Runge-Kutta type methods, the deviation increases with the time step but it is still considerably less than the global error in the ℓ_2-norm.

B. Interference pattern for a three-level system

To further test the different methods, we consider an example of a three-state system (15), with several interfering wave packets. The development of the system is followed over 5200 fs. The ground state is coupled dynamically with the $A\ ^1\Sigma_u^+$ state by a sequence of laser pulses and the $A\ ^1\Sigma_u^+$-state is (statically) spin-orbit coupled to the $b\ ^3\Pi_u$ state. The laser pulses are chosen such that every second pulse causes a negative interference with the wave packet approaching the Franck-Condon region. The spin-orbit coupling will cause a build up of probability on the $b\ ^3\Pi_u$ state causing a complex interference pattern.

Figure 4 shows the probability distribution for the $A\ ^1\Sigma_u^+$ state. The phase and timing of the pump pulses were chosen such that every second pulse causes the population on the A state to almost vanish due to negative interference. Figure 5 show the simultaneous dynamics on the spin-orbit coupled $b^3\Pi_u$ state. The surfaces cross at $r=5.1$ Å, and the wave packet on the A state will thus pass the crossing point with the b state twice per each period, leading to several interfering wave packets.

We compare the performance of the split operator with the two fourth-order methods M/L 4 and PRK4. The result for the population of the third state and the cross correlation with the eigenstate of the third state can be seen in Figs. 6 and 7. We note that the performance of the various methods

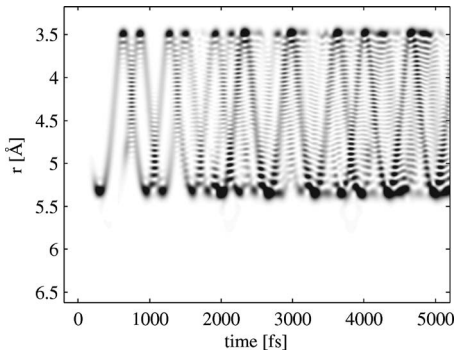

FIG. 5. Probability distribution for the $b\ ^3\Pi_u$ state.

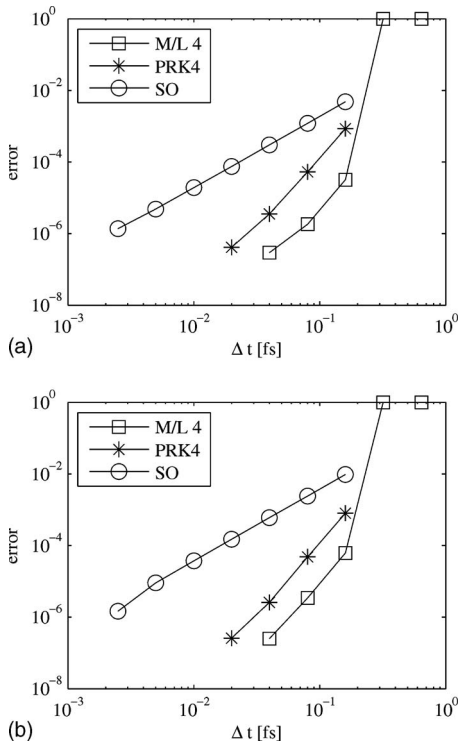

FIG. 6. Accuracy of the different methods. (a) Cross-correlation function. (b) Population.

resembles the observations from our first example. There is yet a difference concerning stability: The PRK4 method becomes unstable for $\Delta t \approx 0.2$ fs. Also in the case of the Magnus-Lanczos propagator, we can clearly see the region where the Lanczos algorithm with $p=5$ is outside the super-

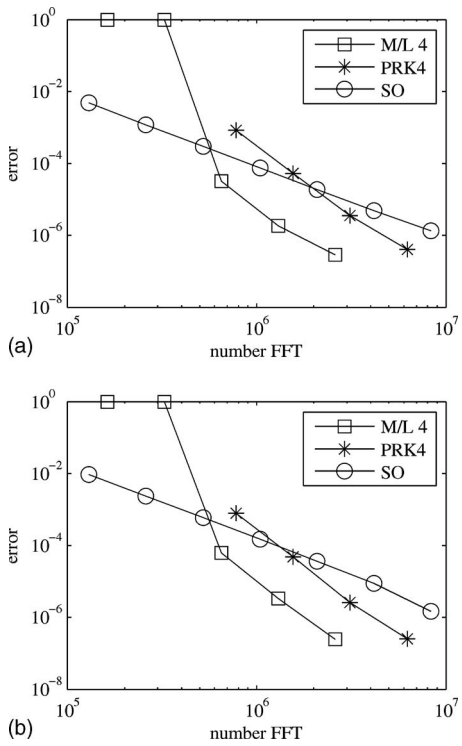

FIG. 7. Efficiency of the different methods. (a) Cross-correlation function. (b) Population.

linear convergence range. Hence, one should chose a larger Krylov space when doing low-accuracy computations with the Magnus-Lanczos algorithm.

VI. SUMMARY AND CONCLUSIONS

To accurately simulate the outcome of quantum dynamical experiment with explicitly time-dependent Hamiltonians, accurate and efficient propagator methods must be used. In this paper, the numerical solution of the explicitly time-dependent Schrödinger equation has been studied with the focus on Hamiltonians arising from light-molecule interaction. The RWA for a two-state system is analyzed using the Magnus expansion to represent the solution analytically, yielding an expression for the leading error term of the RWA modeling. For a laser pulse with a Gaussian envelope function, the quality depends on the strength of the pulse and the period of the oscillation. The analysis shows that the RWA modeling improves the quality of the solution for time steps larger than a half period of the laser pulse. However, a systematic error is introduced on the scale of this period which is why the error flattens out.

For computations with the full time dependence of the Hamiltonian, geometrical and exponential integrators were compared. For low-accuracy calculations, a simple second-order split-operator is quite competitive. For more accurate computations, however, we show that higher order methods are more efficient. Among the exponential integrators, a fourth-order accurate truncation of the Magnus expansion representation of the propagator stands out under the assumption that coupling between each two energy surfaces is not time and space dependent at the same time. This method has a small error constant compared to equally ordered partitioned Runge-Kutta schemes and is relatively easy to evaluate after simplifying the commutators analytically. For higher order, the Magnus approximation becomes quite complicated and is thus less competitive.

Geometric numerical integrators with optimized coefficients as proposed in Ref. 15 have been shown to be efficient in our computations as well. The partitioned Runge-Kutta methods captivate because of their generality: The implementation is rather independent of the Hamiltonian and the order as well as the coefficients can be varied yielding a family of different methods. Furthermore, in the form as discussed in this paper the method is memory efficient since only one vector of the real and the imaginary parts, respectively, is needed. This is especially advantageous for computations in higher dimensions.

A drawback of geometric numerical integration is though the fact that the symplecticity of the method disappears when using a straightforward adaptive time stepping (cf.Ref. 35). Another disadvantage of PRK methods is the limited stability domain for the time step.

In summary, the split-operator method should only be used when low accuracy is acceptable. For accurate and efficient time stepping, the Magnus-Lanczos approach appears to be the best choice.

Future work includes extending the study to higher dimensions as well as applying the result to laser assisted control of chemical reactions.

[1] A. H. Zewail, *Femtochemistry* (World Scientific, Singapore, 1994).
[2] C. Leforestier, R. H. Bisseling, C. Cerjan, M. D. Feit, R. Friesner, A. Guldberg, A. Hammerich, G. Jolicard, W. Karrlein, H.-D. Meyer, N. Lipkin, O. Roncero, and R. Kosloff, J. Comput. Phys. **94**, 59 (1991).
[3] C. Lubich in *Quantum Simulation of Complex Many-Body Systems: From Theory to Algorithms*, edited by J. Grotendorst, D. Marx, and A. Muramatsu (John von Neumann Institute for Computing, Jülich, 2002), p. 459.
[4] D. J. Tannor, *Introduction to Quantum Mechanics: A Time-Dependent Perspective* (University Science Books, Sausalito, 2007).
[5] J. M. Sanz-Serna and A. Portillo, J. Chem. Phys. **104**, 2349 (1996).
[6] P. Schwendner, F. Seyl, and R. Schinke, Chem. Phys. **217**, 233 (1997).
[7] W. Magnus, Commun. Pure Appl. Math. **7**, 649 (1954).
[8] A. Iserles, H. Z. Munthe-Kaas, S. P. Nørsett, and A. Zanna, Acta Numerica **9**, 215 (2000).
[9] I. I. Rabi, Phys. Rev. **51**, 652 (1937).
[10] B. C. Hall, *Lie Groups, Lie Algebras, and Representations* (Springer, New York, 2003).
[11] U. Peskin, R. Kosloff, and N. Moiseyev, J. Chem. Phys. **100**, 8849 (1994).
[12] S. K. Gray and J. M. Verosky, J. Chem. Phys. **100**, 5011 (1994).
[13] R. J. Littlejohn, Phys. Rep. **138**, 193 (1986).
[14] E. Hairer, C. Lubich, and G. Wanner, *Geometric Numerical Integration: Structure-Preserving Algorithms for Ordinary Differential Equations* (Springer-Verlag, Berlin, 2004).
[15] S. Blanes and P. C. Moan, J. Comput. Appl. Math. **142**, 313 (2002).
[16] S. Blanes, F. Casas, and A. Murua, J. Chem. Phys. **124**, 234105 (2006).
[17] S. K. Gray and D. E. Manolopoulos, J. Chem. Phys. **104**, 7099 (2006).
[18] R. I. McLachlan, SIAM J. Sci. Comput. (USA) **16**, 151 (1995).
[19] M. D. Feit and J. A. Fleck, J. Chem. Phys. **78**, 301 (1983).
[20] G. Strang, SIAM (Soc. Ind. Appl. Math.) J. Numer. Anal. **5**, 506 (1968).
[21] S. Blanes, Appl. Numer. Math. **37**, 289 (2001).
[22] R. I. McLachlan and G. R. W. Quispel, Acta Numerica **11**, 341 (2002).
[23] S. Blanes, F. Casas, and A. Murua, Found. Comput. Math., Report No. NA2006_08, 2006.
[24] S. Blanes and P. C. Moan, Phys. Lett. A **295**, 35 (2000).
[25] T. J. Park and J. C. Light, J. Chem. Phys. **85**, 5870 (1986).
[26] J. W. Demmel, *Applied Numerical Linear Algebra* (SIAM, Philadelphia, 1997).
[27] M. Hochbruck, C. Lubich, and H. Selhofer, SIAM J. Sci. Comput. (USA) **19**, 1552 (1998).
[28] H. Tal-Ezer, R. Kosloff, and C. Cerjan, J. Comput. Phys. **100**, 179 (1992).
[29] S. Blanes, F. Casas, and J. Ros, BIT Numerical Mathematics **40**, 434 (2000).
[30] N. Gador, B. Zhang, H. O. Karlsson, and T. Hansson, Phys. Rev. A **70**, 033418 (2004).
[31] S. Blanes and P. C. Moan, Appl. Numer. Math. **56**, 1519 (2006).
[32] P. Pechukas and J. C. Light, J. Chem. Phys. **44**, 3897 (1966).
[33] M. Hochbruck and C. Lubich, SIAM (Soc. Ind. Appl. Math.) J. Numer. Anal. **41**, 945 (2003).
[34] S. J. Park, S. W. Suh, Y. S. Lee, and G.-H. Jeung, J. Mol. Spectrosc. **207**, 129 (2001).
[35] J. M. Sanz-Serna and M. P. Calvo, *Numerical Hamiltonian Problems* (Chapman and Hall, London, 1994).